Numerical study of the sputtering in a dc magnetron

Ivan Kolev[a] and Annemie Bogaerts[b]
Department of Chemistry, Research group PLASMANT, University of Antwerp, Universiteitsplein 1, 2610 Antwerp, Belgium

(Received 14 July 2008; accepted 13 October 2008; published 8 December 2008)

In this article, the process of sputtering and the behaviour of the sputtered atoms in a dc magnetron is studied by means of numerical simulations. The proposed model is a self-consistent approach, based on the particle-in-cell-Monte Carlo collision method. In this way, the process of sputtering is treated self-consistently with respect to the other processes in the magnetron plasma. The studied pressure range is 1–100 mtorr. The effects of the target-substrate distance and the choice of the scattering angle in the collisions between sputtered atoms and background gas atoms are also discussed. © *2009 American Vacuum Society.* [DOI: 10.1116/1.3013856]

I. INTRODUCTION

Magnetron sputter deposition has established itself as one of the major techniques for deposition of both metallic and nonmetallic thin films on various substrates. The main efforts in the process of deposition are toward the quality of the film and the amount of the deposition in terms of rate and coverage area. Both are determined from quantities such as the spatial, angular, and energetic distribution of both neutral gas and sputtered atoms that arrive at the substrate.[1,2] The factors that determine these distributions are the initial angular and energy distribution of the sputtered atoms at the cathode, and the collision processes of sputtered and neutral gas atoms in the discharge. These are, in their turn, dependent on the energy and angular distribution of the bombarding particles at the cathode (atoms and ions) and on the operating conditions, such as gas pressure and temperature, gas flow rate, and the applied electrical power. Correspondingly, a comprehensive model should be able to predict the spatial distribution of the particles arriving at the substrate in terms of density, energy, and impinging angle by accounting correctly for the above mentioned processes and conditions.

So far, many attempts have been made to model the transport of the sputtered species.[3–12] They are primarily based on the Monte Carlo technique. Monte Carlo simulations are popular due to the fact that they are relatively easy for programming and offer a particle (kinetic) approach. The latter is required from the operating conditions of sputter magnetrons (pressure in the millitorr range) and from the need to obtain detailed distributions at the substrate, as discussed above. The Monte Carlo approach is also suitable because the transport of the sputtered atoms across the discharge is not directly influenced by the electric field and therefore there is no need to include a field solver. There is, however, one significant drawback. An initial guess for the spatial, energy, and angular distribution of the sputtered atoms at the cathode is necessary. Due to the highly localized plasma in the magnetrons, the erosion on the target is also highly localized. An exact representation of this localization in a Monte Carlo simulation is problematic. One possible way is to have measured erosion profiles that can be used for obtaining the starting positions of the sputtered atoms at the cathode. This, however, weakens the advantage of modeling, because a prior experiment is needed. In addition, the essential physical principle for detailed equilibrium, giving the connection between the energy of the particle bombarding the cathode (related to the discharge voltage and pressure) and the initial energy of the sputtered particle cannot be obeyed. Other possible important phenomena, such as, ionization of the sputtered atoms with corresponding self-sputtering and gas inhomogeneity caused by gas heating[13] are difficult to implement and usually disregarded. To overcome all these uncertainties, a self-consistent modeling is needed. This means that not only the transport of the sputtered species in the discharge is resolved but also their initial state in terms of position and velocity is included as a function of the discharge parameters and processes.

In the present article, the results of such a self-consistent model, applied to the sputtered atoms in a dc planar magnetron, will be discussed.

II. DESCRIPTION OF THE MODEL

The present model is based on the general particle-in-cell/Monte Carlo collision (PIC/MCC) algorithm.[14] The model includes the following plasma species: electrons, argon ions (Ar^+), sputtered copper atoms, singly ionized copper ions (Cu^+), argon fast atoms, and argon metastable atoms. The last are included for their role in the production of copper ions. The collision processes among these species are also considered based on cross sections from literature. All of the details of the model can be found elsewhere.[15,16] Here, a brief summary of the main features with respect to the sputter-deposition process is given only.

All above mentioned plasma species are represented by so-called superparticles.[14] Each superparticle represents a large number of real particles. This number is known as their weight. In the code, the weight is variable, in order to keep the total number of superparticles reasonable. When the number of superparticles exceeds some predefined limit, it is reduced twice and the weight is correspondingly doubled so

[a]Electronic mail: ivan.kolev@ua.ac.be
[b]Electronic mail: annemie.bogaerts@ua.ac.be

that the real plasma density stays unchanged. This limit has been set to 10^6 per species in the present study.

The model incorporates an external electrical circuit, consisting of a ballast resistor and an ideal voltage source. The meaning of the circuit is to stabilize the simulation in the desired part of the current-voltage characteristic of the magnetron. The necessity for the presence of the circuit has been motivated elsewhere.[17–19] The practical details for the implementation in the model are given in.[16,19]

Sputtering is included based on the semiempirical approach[20] giving the sputtering yield, Y, as a function of the energy of the bombarding particle, E,

$$Y(E) = 0.42\frac{\alpha^* QKs_n(\varepsilon)}{U_s[1 + 0.35U_s s_e(\varepsilon)]}[1 - (E_{\text{ih}}/E)^{1/2}]^{2.8}.$$

Here, U_s is the sublimation energy of the cathode material, E_{th} is the threshold energy of the process, and ε is the reduced energy. The rest of the symbols are material dependent. Their exact meaning and values can be found in Ref. 20.

The initial velocity of the sputtered atoms is sampled from the Sigmund-Thompson differential distribution[21–23] for the sputtered flux

$$\frac{d^3\Phi}{dEd^2\Omega} \propto \frac{E}{(E + U_b)^{3-2m}}\cos\Theta,$$

where E is the energy of the sputtered atom, U_b is the surface binding energy, and Θ is the polar angle of the emitted particles with respect to the surface normal. Typically, U_b is taken to be equal to the heat of sublimation. The value of m is an energy-related parameter in the differential cross section used for a screened Coulomb potential and varies from $m=0.5$ at incident energies around 100 keV for Ar–Cu down to $m=0$ for low energies.[21] Thus, $m=0$ is a good approximation for the problem of interest (i.e., typical incident energies of a few hundreds of eV at maximum).

The validity of the Sigmund-Thompson distribution is limited to sputtered particles with energies small in comparison to the energy transferred in an elastic head-on collision given by

$$E_{\max} = \frac{4M_{\text{inc}}M_{\text{sp}}}{(M_{\text{inc}} + M_{\text{sp}})^2}E_{\text{inc}}. \tag{1}$$

Here, M_{inc} and M_{sp} stand for the masses of the incident ion and sputtered atom, respectively, and E_{inc} is the energy of the bombarding ion.

The velocity of the sputtered atoms is then obtained by performing a random sampling from the Sigmund-Thompson distribution with $m=0$,

$$U_1 = 4\int_0^{\infty}\frac{U_b E}{(E + U_b)}dE\int_0^{\Theta}\sin\Theta'\cos\Theta' d\Theta', \tag{2}$$

$$U_2 = 4\int_0^{E}\frac{U_b E'}{(E + U_b)}dE'\int_0^{\pi/2}\sin\Theta\cos\Theta d\Theta. \tag{3}$$

Here U_1 and U_2 are independent random numbers, homogeneously distributed between zero and one. Equation (2) gives the direction of the initial velocity, by means of the inclination, Θ, from the normal to the cathode surface

$$\cos\Theta = \sqrt{1 - U_1}, \quad \sin\Theta = \sqrt{U_1}. \tag{4}$$

Equation (3), which determines the initial energy of the sputtered atom, leads to a quadratic equation for E, which physical root is

$$E = \frac{U_b\sqrt{U_2}}{(1 - \sqrt{U_2})}. \tag{5}$$

The energy, calculated in Eq. (5) is compared to the maximum allowed energy, $E_{\max}$, given by Eg. (1). If $E > E_{\max}$, E is rejected and a new U_2 is generated. The procedure is repeated until E is accepted. Then the initial speed of the sputtered atoms, c, is obtained from $c=\sqrt{2E/M_{\text{sp}}}$.

The collisions between the sputtered copper atoms and the background argon atoms are treated from theoretical considerations due to a lack of information about experimental cross sections. As a starting point the range concept[24] is used with the interaction potential, V, as a function of the interatomic distance, r, in the form

$$V(r) = Z_{\text{Cu}}Z_{\text{Ar}}q^2a_s^{n-1}\frac{r^n}{n}, \tag{6}$$

where a_s is a parameter known as screening length (to be defined below) and Z_{Cu} and Z_{Ar} are the atomic numbers of Cu and Ar. The power, n, specifies the nature of the interaction. As shown in Ref. 24, the potential Eq. (6) leads to a cross section

$$\sigma(E) = \frac{2\pi}{n-1}a_s^2\beta_n^{1/n}\varepsilon^{-2/n}, \tag{7}$$

where $E=m_{\text{Cu}}v_{\text{Cu}}^2/2$ is the precollision energy of the sputtered atom, $\beta_n=[(3n-1)/8n^2]$, and the reduced energy, ε, is defined as

$$\varepsilon = \frac{a_s M_{\text{Ar}}}{Z_{\text{Cu}}Z_{\text{Ar}}q^2(M_{\text{Cu}} + M_{\text{Ar}})}E. \tag{8}$$

Equation (7) is analytical and universally valid. For practical applications, however, the power, n, must be specified as well as the screening length, a_s. Sielanko[25] proposed a numerical fit of n as a function of the reduced energy, ε,

$$n(\varepsilon) = 1 + 4\exp(-1.9\varepsilon^{0.1}). \tag{9}$$

The screening length is taken in Firsov's approximation[26]

$$a_s = \frac{0.8853a_0}{(Z_{\text{Cu}}^{1/2} + Z_{\text{Ar}}^{1/2})^{2/3}}, \tag{10}$$

where the number 0.8853 is the evaluation of the Thomas-Fermi constant, which exact value is $(9\pi^2)^{1/3}2^{-7/3}$ and $a_0=0.529$ Å is the Bohr radius.

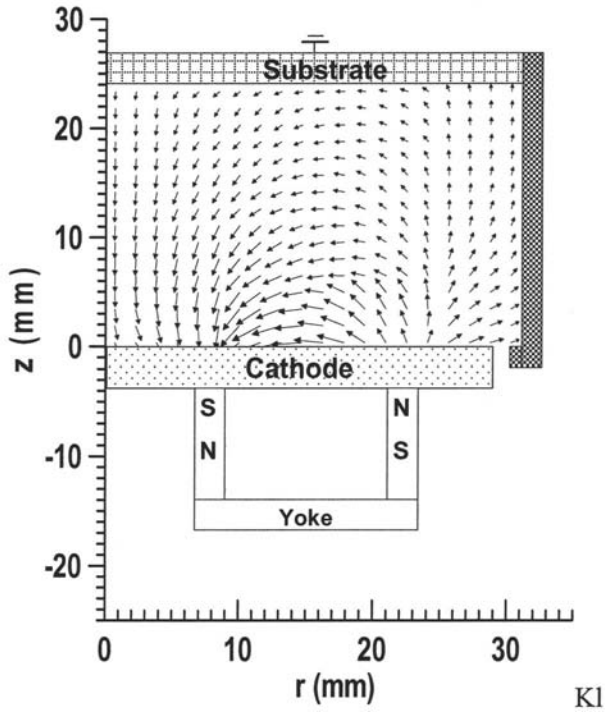

FIG. 1. Scheme of the sputter magnetron considered in the model. The magnetron is axially symmetrical towards the axis $r=0$. The magnetic field lines are also drawn.

The above approach allows determining the scattering angle, χ. As shown in Ref. 25,

$$\cos\chi = 1 - 2\left[1 + \frac{b_\chi^2 \varepsilon^{2/n}}{a_s^2 \beta_n^{1/n}}\right]^{-n}. \tag{11}$$

To determine the impact parameter b_χ in Eq. (11), the total cross section is presented as $\sigma(E)=\pi b_0^2$, where b_0 is the maximum value of the impact parameter. This approach was proposed by Wronski.[27] Then, a random sampling is performed

$$U = \int_0^{b_\chi} \frac{2\pi b'}{\pi b_0^2} db', \quad U \in [0,1],$$

resulting in

$$b_\chi = \sqrt{\frac{U\sigma(E)}{\pi}}, \tag{12}$$

with $\sigma(E)$ calculated from Eq. (7).

III. RESULTS AND DISCUSSION

In this study, a planar dc magnetron operated in argon and with a copper cathode is investigated. Its scheme is shown in Fig. 1. It is a Von Ardenne PPS 50 magnetron (commercially available), used with plasma shield (the sidewall on the scheme in Fig. 1). The axisymmetric magnetic field is created by two concentric magnets located under the powered electrode—the cathode. All walls, except the cathode, are grounded and act as an anode. The smallest separation between the electrodes is equal to 2 mm. The magnetic field used in the simulation has been experimentally measured when the discharge was not operational.[28] The simulations are performed in a constant power regime of about 160 W. The deviation from that value did not exceed 7%. Calculations for a pressure in the range 1–100 mtorr are presented.

A. Bombarding fluxes at the cathode

The heavy particles that bombard the cathode are the argon ions and atoms and the copper ions. Some copper atoms can also return to the cathode, but their energy is normally below the threshold for sputtering.

The calculated bombarding fluxes of the Ar atoms, Ar^+ ions, and Cu^+ ions for different pressures are shown in Figs. 2(a)–2(c), respectively. The bombarding fluxes of all types of particles are localized in the region, where the radial component of the magnetic field is strongest, i.e., around $r=18$ mm (see Fig. 1). The flux of the Ar^+ ions [see Fig. 2(b)] is most localized in the radial direction, followed by those of the Cu^+ ions [Fig. 2(c)]. The flux of Cu^+ ions is more spread, because of the fact that a fraction of the Cu^+ ions is produced by Penning ionization, which is not as localized as the electron-impact ionization. The latter is almost entirely responsible for the creation of the Ar^+ ions.

The flux of Ar atoms [Fig. 2(a)], although with a maximum approximately identical to the Ar^+ flux, spreads over the entire cathode (the target). The localized part of the flux originates from symmetric charge transfer collisions, whereas the part that is located outside of the maximum is related to Ar–Ar elastic collisions.

The magnitudes of the Ar^+ and Ar fluxes are very close, whereas the magnitude of the Cu^+ flux is almost two orders of magnitude lower. The latter corresponds to the ratio of the densities of the argon gas and the copper atoms in the discharge.

The maximum of the Ar^+ flux first increases with pressure (the maximum calculated value corresponds to $p=4$ mtorr) and then decreases, while at the same time the flux becomes more spread in the radial direction [see Fig. 2(b)]. This trend can be explained with the increase in the ionization rate with pressure at low pressures. At higher pressures, the rate of the symmetric charge exchange collisions plays a more significant role and neutralizes the effect of the increased ionization.

Similar is the picture for the Ar atom flux [see Fig. 2(a)]. The maximum of their flux at the cathode, however, corresponds to $p=25$ mtorr. The flux of Cu^+ ions, on the other hand, increases with pressure in the entire pressure range because the total amount of sputtering increases.

B. Energies of the bombarding species

As it has already been mentioned, the sputtering is also a function of the energies of the bombarding fluxes. For that reason, the calculated mean energies of the bombarding Ar atoms and Ar^+ ions are presented in Figs. 3(a) and 3(b), respectively. The mean energy of the Cu^+ ions (not presented here) has a similar radial distribution. However, its maximal

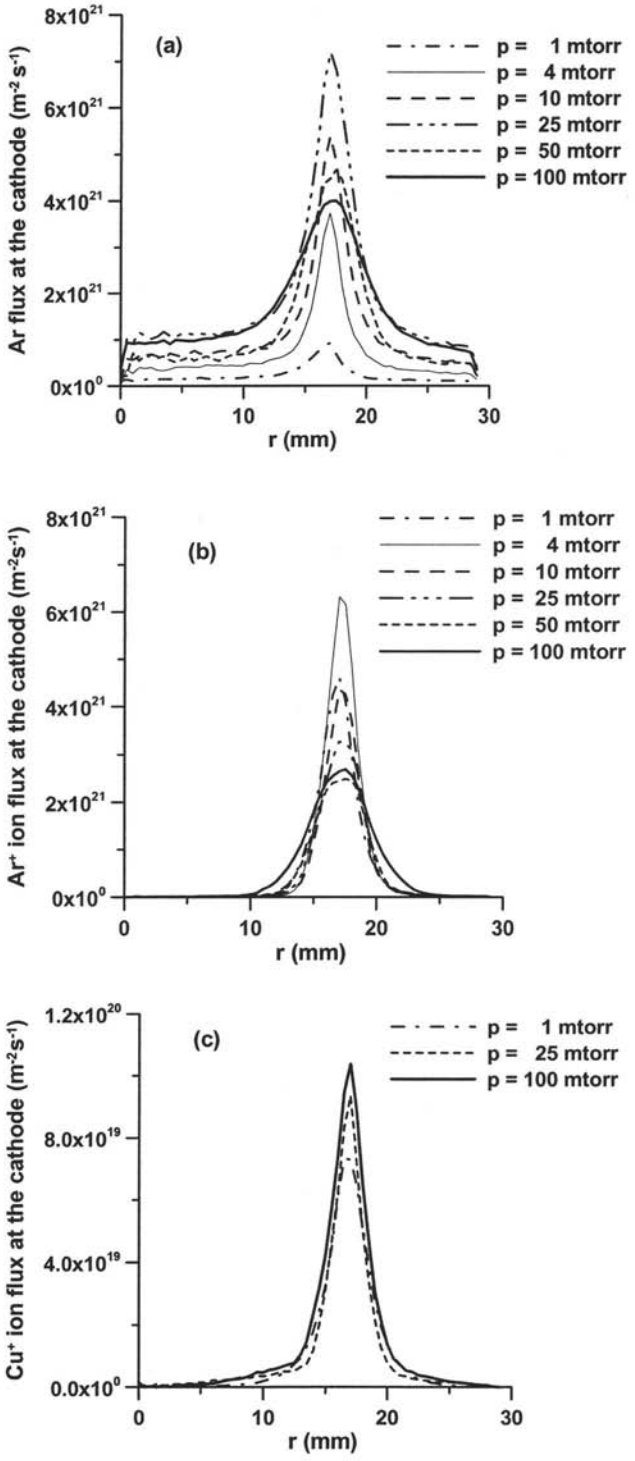

FIG. 2. Calculated flux at the cathode for different values of the gas pressure. (a) fast Ar atoms (as fast atoms are considered those, which energy is above the sputtering threshold energy), (b) Ar^+ ions and (c) Cu^+ ions.

values are only slightly lower than the applied potential. This is in accordance with the results obtained for a hollow cathode discharge[29] and represents the difference in the cross section of the elastic scattering of Ar^+ and Cu^+ from Ar as well as the difference in mass between Cu^+ and Ar^+.

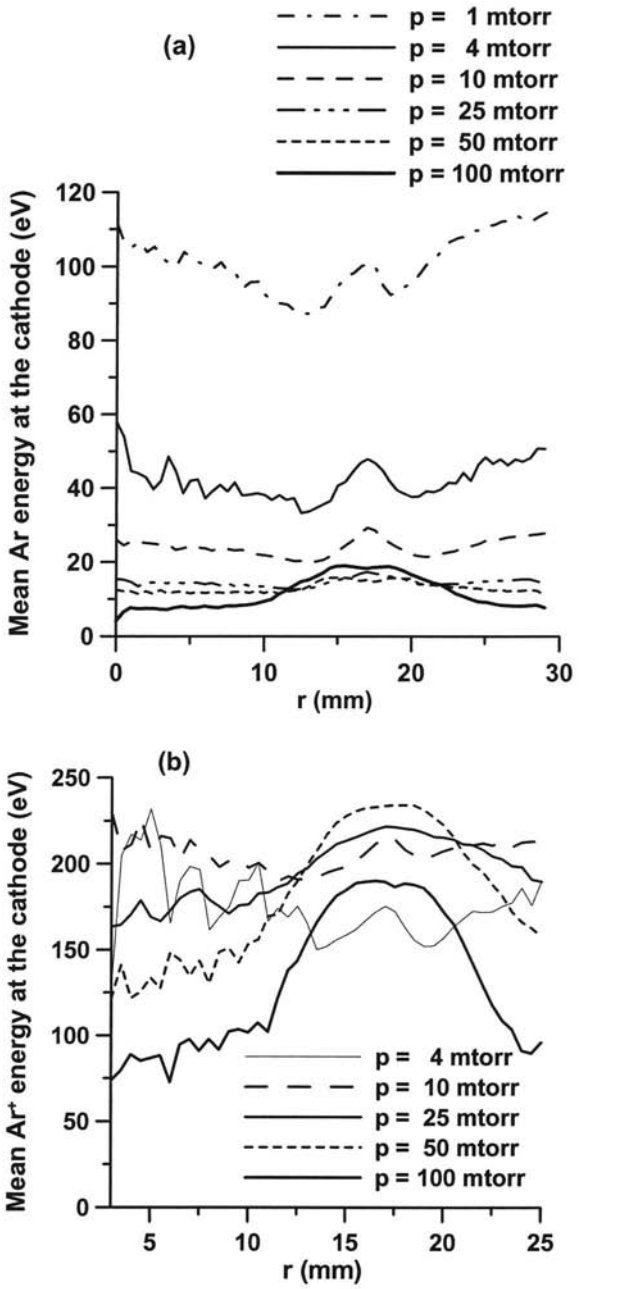

FIG. 3. Calculated distribution of the mean energy at the cathode for different values of the pressure: (a) Ar atoms and (b) Ar^+ ions. The mean Ar^+ energy for $p=1$ mtorr is very similar to that for $p=4$ mtorr and is omitted for clarity.

The mean Ar atom energy decreases from about 100 eV at $p=1$ mtorr to about 16 eV at pressures above 25 mtorr, above the racetrack. It is natural to expect that the mean energy will decrease more or less monotonically with the rise of pressure due to the increasing probability for elastic collisions. The fact that the mean energy is approximately the same in the pressure range 25–100 mtorr can be attributed to the fact that at these pressures gas heating becomes significant[15] and the gas density remains more or less constant at rising pressure (due to the increased temperature). As a consequence, the energy lost due to collisions is more or less the same.

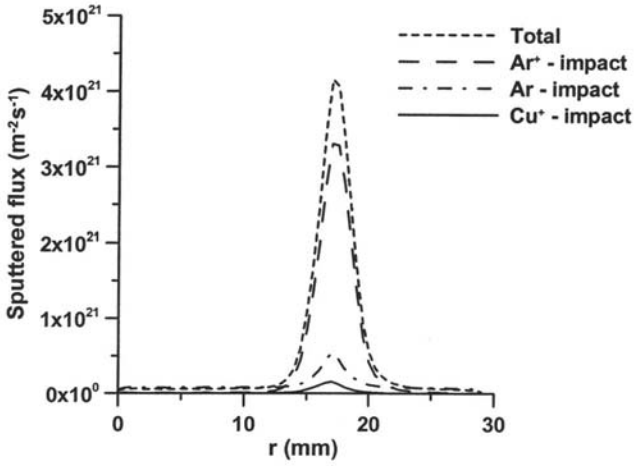

FIG. 4. Calculated contribution of the different species to the sputtering flux from the cathode for $p=10$ mtorr.

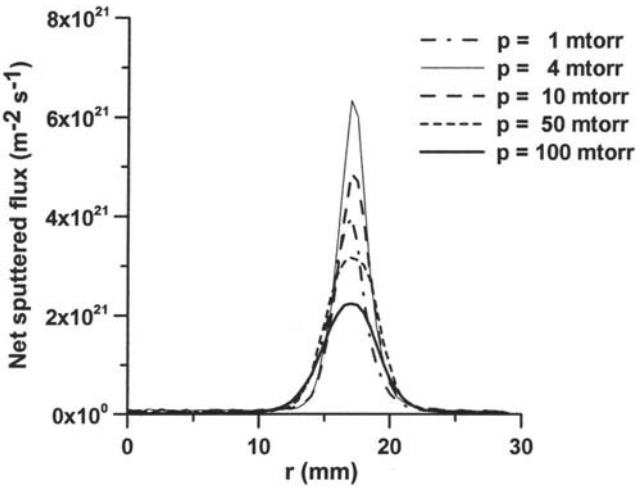

FIG. 5. Calculated net sputtered flux from the cathode for different values of the gas pressure. The data for $p=25$ mtorr is omitted for clarity.

It is clear from Fig. 3(a) that at pressures of 25 mtorr and above, the Ar atoms are not expected to have a significant influence on the sputtering, although their flux at the cathode is approximately of the same magnitude as that of the Ar^+ ions [see Figs. 2(a) and 2(b)].

The Ar^+ ions, however, possess enough energy at all pressures studied here for efficient sputtering of the target. The same is true for the Cu^+ ions, but since their flux is about 100 times lower than the Ar^+ flux, it is expected that the Cu^+ ions will have very little importance for the sputtering at the studied operating conditions.

The calculated contribution of the different bombarding species to the sputtering process is presented in Fig. 4 for $p=10$ mtorr. These results are representative for all pressures. The most efficient sputtering is caused by the Ar^+ ions, which are responsible for 83% of the sputtered copper atoms. The contribution of Ar atoms is about 13%, whereas the Cu^+ ions contribute only for about 4% of the total sputtering.

C. Sputtered flux from the cathode

When calculating the sputtered flux from the cathode, the Cu atoms that return at the cathode as a result of elastic collisions are considered adsorbed and counted with a minus sign in the sputtered flux. Therefore, the calculated sputtered flux is the net flux equal to the number of the sputtered atoms minus the number of the returned (redeposited) atoms. It is shown in Fig. 5 for different values of the pressure. The net flux is at maximum at $p=4$ mtorr and has a maximum value of 6.3×10^{21} m^{-2} s^{-1}, which is about 50% more than the maximum value at $p=1$ mtorr. With further increase in the pressure, the maximum of the sputtered flux decreases and at $p=100$ mtorr it is one-third of that at $p=4$ mtorr. The maximum at $p=4$ mtorr is related to the fact that the Ar^+ flux has a maximum at this pressure [see Fig. 2(b)]. With the increase in the pressure, the sputtered flux becomes more spread in the radial direction, which can lead to better utilization of the target. However, when the choice is for most intensive sputtering, the optimal pressure range appears to be 1–10 mtorr.

Based on the value of the net sputtered flux from the cathode, the erosion profile can be calculated. To validate the calculated results, the erosion profile at $p=10$ mtorr is calculated and compared to the experimentally measured erosion profile for similar pressure ($p_{exp}=10.65$ mtorr).[28] Both normalized profiles are shown in Fig. 6.

The comparison shows very reasonable agreement. The location of the measured and calculated erosion craters coincides within 0.3 mm. This can easily be attributed to the possible error in the measurement of the magnetic field, which is an input for the model. The central part of the crater agrees also very well. Some deviation in the erosion depth is observed at the periphery of the crater. The measurements

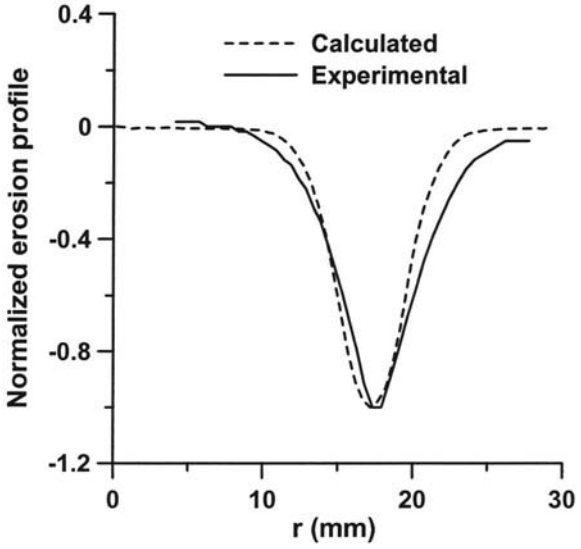

FIG. 6. Calculated (dashed line) and measured (solid line) normalized erosion profiles for $p=10$ mtorr.

show some net redeposition in the region, $r<8$ mm, which is not predicted by our results. This fact, as well as the generally smaller agreement in the periphery of the crater provokes a discussion about the collision cross section of the Cu–Ar elastic collisions and the scattering angle in the Ar–Ar collisions, which may influence the directionality of the argon atoms. However, as a whole, the agreement can be considered to be satisfactory for validating the model.

In other types of discharges, such as analytical glow discharges and hollow cathode discharges, where sputtering also takes place, it has been reported that significant redeposition of the sputtered atoms can occur. In the first group of discharges, a redeposition of 57% has been calculated[30,31] at a pressure of 75 Pa. In the second group, the redeposited atoms have been calculated even to exceed the sputtered atoms at given areas of the cathodes[32] at a pressure of 300 mtorr. At our operating conditions (i.e., $p<100$ mtorr), the rate of redeposition, caused by backdiffusion, is much lower. Our calculations predict that it is at maximum about 7% of the total sputtered flux (i.e., at $p=100$ mtorr). At $p=1$ mtorr, it is only 0.1%.

D. Calculated density profiles of the sputtered atoms

After being sputtered from the cathode, the copper atoms are transported towards the substrate and the sidewall of the magnetron chamber. Their movement is inertial, with changes in the velocity only due to collisions.

The calculated density profiles for pressures of 4, 25, and 100 mtorr are presented in Figs. 7(a)–7(c), respectively. At $p=4$ mtorr, the distribution of the sputtered atoms in the volume of the discharge, away from the cathode, is relatively homogeneous because the pressure is too low for enough collisions that can act as an obstruction for the Cu transport. The maximum near the cathode represents the ejection source. The situation at $p=10$ mtorr (not shown here) is identical. This is in full agreement with other simulation works for magnetron sputtering at the same pressure range.[8,33]

At $p=25$ mtorr, the copper transport is already influenced by the collisions [see Fig. 7(b)], but the peak density in the volume is still lower than the density near the target. This situation is changed at $p=100$ mtorr; where the peak density inside the discharge is higher than the density near the target, as illustrated in Fig. 7(c). At this pressure, the transport of the sputtered atoms is already collision dominated. The pictures at $p=10$ mtorr and $p=50$ mtorr, both not shown here, are transitional with respect to the results presented here.

E. Deposition flux at the substrate

The flux of sputtered atoms at the substrate (i.e., the deposition flux) calculated for several values of the gas pressure is plotted in Fig. 8(a). It is clearly pressure dependent. An increase in the pressure leads to a decrease in the flux. The maximum values of the flux, which are located in the middle of the substrate for all pressures, differ by a factor of 3, for a pressure difference in two orders of magnitude

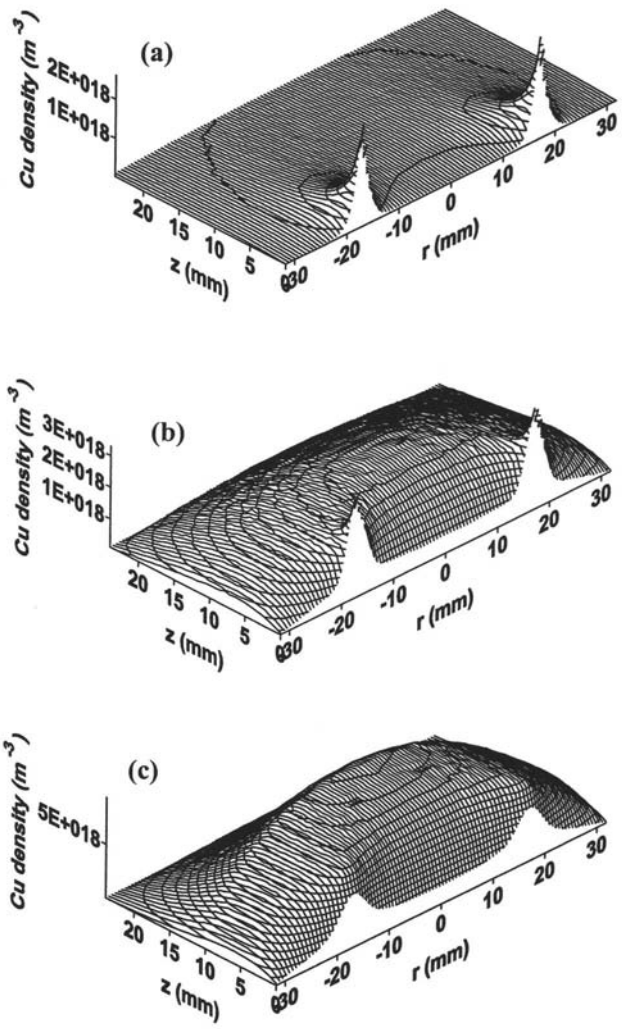

FIG. 7. Calculated Cu atom density profile for: (a) $p=4$ mtorr, (b) $p=25$ mtorr, and (c) $p=100$ mtorr.

(1–100 mtorr). At the same time, the spatial inhomogeneity of the flux with respect to the radial coordinate, defined as the ratio of the flux in the center of the substrate and in its periphery, does not change with pressure, except for the case of $p=100$ mtorr, which appears to be less inhomogeneous than at the lower pressures.

The mean energy of the arriving particles also decreases with increasing pressure, as can be seen in Fig. 8(b). The value of the mean energy drops from 18.3 eV at $p=1$ mtorr to 12 eV at $p=100$ mtorr. The relatively high values of the mean energy arise from the asymmetry of the energy distribution of the sputtered atoms. This means that there is a small fraction in the energetic tail of the distribution, whereas the majority of the sputtered atoms have much lower energies. This is illustrated in Fig. 9, where the normalized energy distribution of the sputtered atoms at the substrate is plotted for $p=10$ mtorr. The plot is representative for the rest of the pressure values under study. As seen in Fig. 9, the maximum of the distribution is around 3 eV, but there are also atoms arriving at the substrate with energies up to 200 eV.

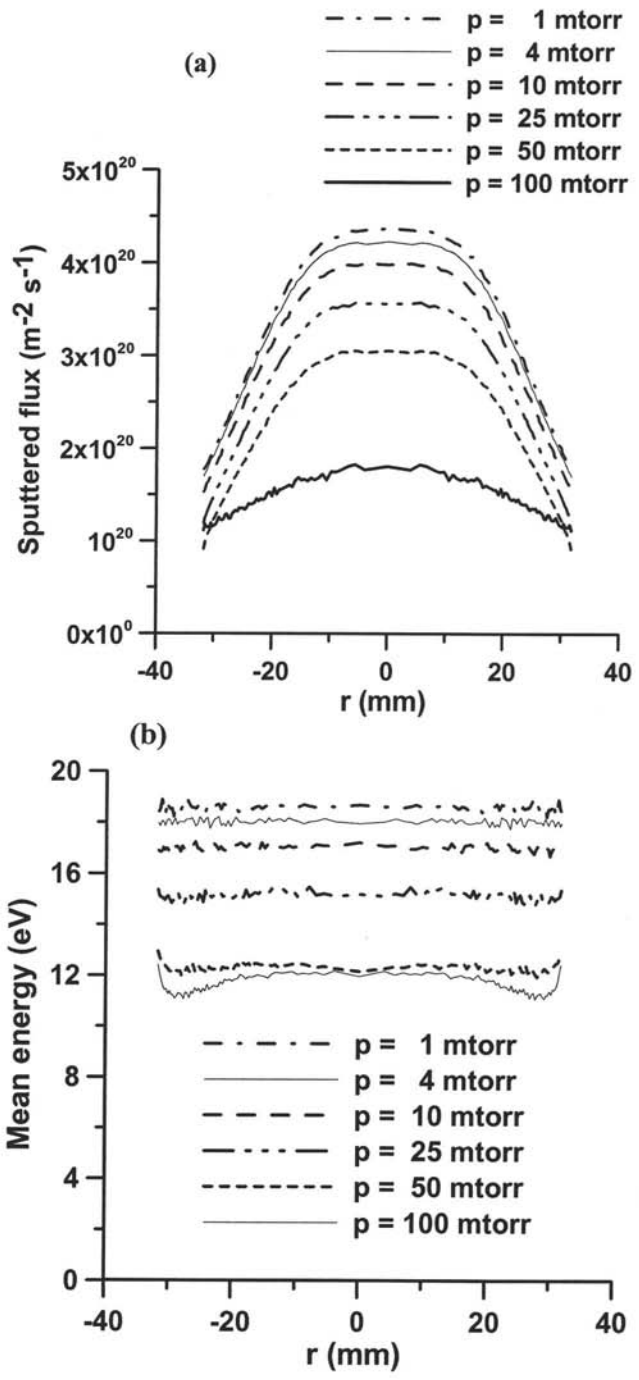

FIG. 8. Calculated flux (a) and mean energy (b) of the sputtered atoms arriving at the substrate for different values of the gas pressure.

F. Influence of the target-substrate distance

The distance between the target and the substrate can affect the quality of the deposited film, by the number of collisions in the plasma, and hence the energy and velocity distribution, of the sputtered atoms. To investigate the importance of this effect, simulations for four distances (24, 50, 100, and 150 mm) have been performed for different values of the pressure. The calculated sputtered flux at the substrate for the four distances at $p=4$ mtorr is presented in Fig. 10. It appears that when enlarging the distance from 24 to 150 mm, the magnitude of the sputtered flux decreases from 4×10^{20} to about 2.4×10^{19} m^{-2} s^{-1}, i.e., more than an order of magnitude. The radial homogeneity of the flux, however, improves by a factor of 1.8. The mean energy also decreases, but only by about 20%. These results demonstrate that the target-substrate distance acts similarly to the change of the gas pressure.

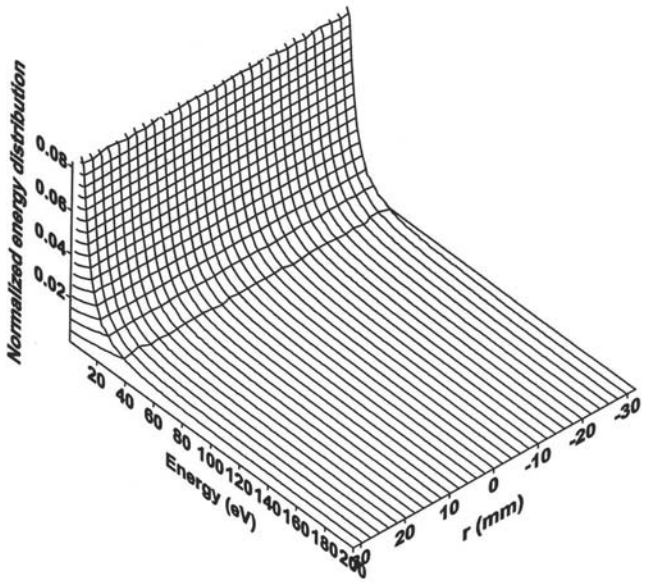

FIG. 9. Calculated normalized energy distribution of the sputtered atoms at the substrate at $p=10$ mtorr.

The same trend holds qualitatively for all pressures. However, the effect of increasing distance on the magnitudes of the sputtered fluxes at the substrate increases with the pressure. At $p=100$ mtorr, the difference in flux for a target-substrate distance of 150 vs 24 mm is already more than three orders of magnitude. Note that at separation $z=150$ mm, the deposited sputtered flux is only 0.01% of the

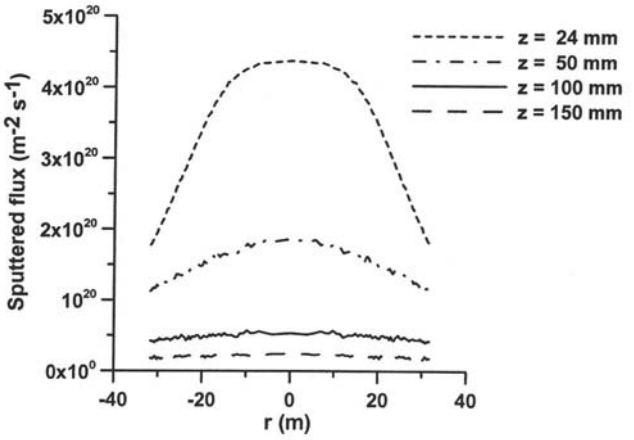

FIG. 10. Calculated sputtered flux arriving at the substrate for different target-substrate separations at $p=4$ mtorr.

originally sputtered flux from the target. It means that almost all sputtered atoms have been scattered towards the sidewall and deposited there, instead of on the substrate.

G. Influence of the scattering angle of Cu atoms on the calculated results

The scattering of argon and copper atoms in the plasma is subject to uncertainty. Not only is the total cross section not precisely known but also the differential cross section that determines the scattering angle. In our study, the scattering angle is considered energy dependent and is calculated according to Eq. (11). A possible alternative is to consider the scattering to be isotropic. This is often applied in simulations when reliable data is not available. In our study, the effect of the choice of scattering angle is investigated by performing three sets of simulations for pressures of 4, 25, and 100 mtorr for a target-substrate separation of 50 mm. Each set consists of two simulations—one with isotropic Cu–Ar scattering and one with scattering treated according to Eq. (11). The results for 4 and 100 mtorr are presented in Figs. 11(a) and 11(b), respectively.

The two ways of treating the scattering lead to a difference in the calculated sputtered flux at the substrate. This difference is calculated to be only 6% at low pressure (4 mtorr), but at higher pressure (100 mtorr) it is already above 100%. At $p=25$ mtorr, it is calculated to be 63% (the results are not shown here).

Therefore, when sputtering is considered at low pressures (below 10 mtorr) the issue of how the scattering angle in the elastic Cu–Ar collisions is treated is of limited importance for the calculation of the sputtered flux at the substrate. At higher pressures, however, the issue should be dealt with carefully.

IV. CONCLUSION

The performed study of a laboratory magnetron Von Ardenne PPS 50 by means of a two-dimensional numerical model, based on the PIC/MCC method, has revealed the generation, transport, and deposition of the sputtered atoms from a copper cathode. The calculated erosion profile agrees very reasonably with the experimentally measured one. The results of the study show that the main sources of sputtering at the examined pressure range, 1–100 mtorr, are the Ar^+ ions. They are responsible for at least 80% of the sputtered atoms at all pressures. The second contributor to the sputtering are the argon atoms, created in symmetric charge transfer between the Ar^+ ions and their parent atoms. The role of self-sputtering (caused by Cu^+ ions) is found to be negligible. The sputtering and deposition efficiency is highest at $p=4$ mtorr. Hence, the most favorable pressure window for sputtering and deposition is found to be within 1 and 10 mtorr.

The distance between the target and the cathode plays a significant role for the efficiency of the deposition, i.e., the radial homogeneity of the deposited film and the deposition rate. The effect of the distance is present at all studied pressures but it is stronger at the highest pressure.

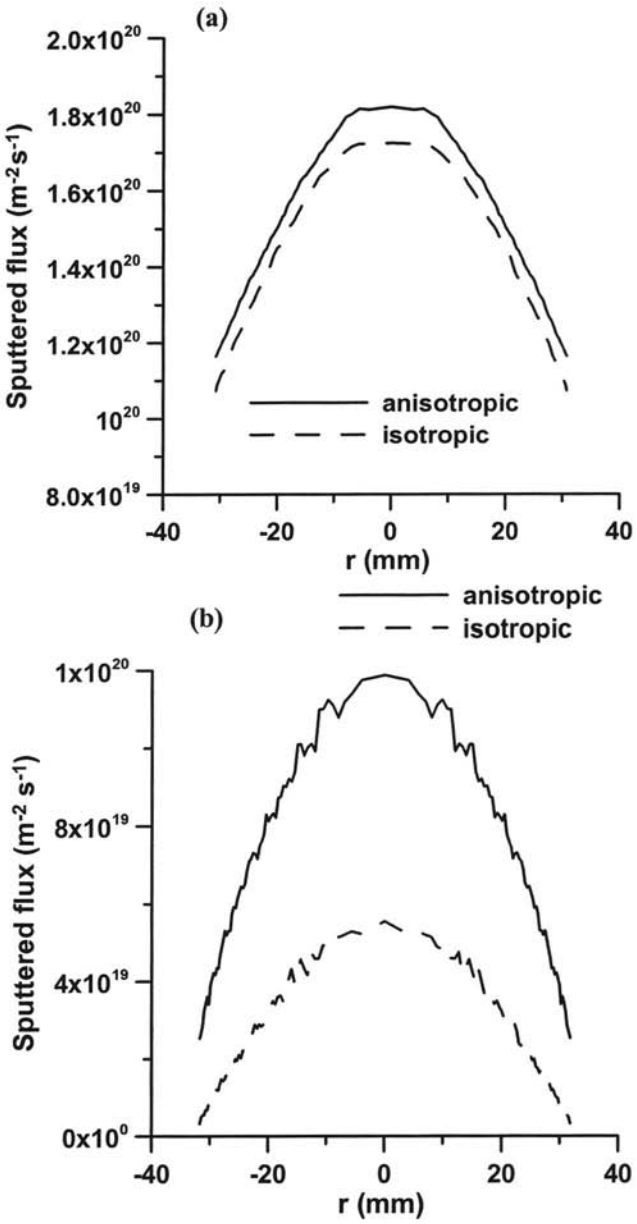

FIG. 11. Calculated sputtered flux at the substrate for a distance of 50 mm between the cathode and the substrate. The solid line represents anisotropic scattering, according to Eq. (11). The dashed line represents isotropic scattering: (a) at $p=4$ mtorr and (b) at $p=100$ mtorr.

Finally, the effect of how the Cu–Ar elastic scattering is treated has been investigated by comparing an energy dependent scattering angle to isotropic scattering. It has been calculated that at lower pressures the difference in the deposited flux is below 10%, whereas at higher pressures it can be above 100% (i.e., a factor of 2).

ACKNOWLEDGMENTS

The calculations were performed on the CALCUA supercomputer facilities of the University of Antwerp. The authors thank N. Baguer and R. Gijbels for the interesting discussions.

[1]I. Petrov, A. Myers, J. E. Greene, and J. R. Abelson, J. Vac. Sci. Technol. A **12**, 2846 (1994).
[2]I. Ivanov, P. Kazansky, L. Hultman, I. Petrov, and J. E. Sundgren, J. Vac. Sci. Technol. B **12**, 314 (1994).
[3]E. Shidoji, M. Nemoto, T. Nomura, and Y. Yoshikawa, Jpn. J. Appl. Phys., Part 1 **33**, 4281 (1994).
[4]Y. Yamamura and M. Ishida, J. Vac. Sci. Technol. A **13**, 101 (1995).
[5]C. Eisenmenger-Sittner, R. Beyerknecht, A. Bergauer, W. Bauer, and G. Betz, J. Vac. Sci. Technol. A **13**, 2435 (1995).
[6]V. Serikov and K. Nanbu, J. Vac. Sci. Technol. A **14**, 3108 (1996).
[7]S. Ido, M. Kashiwagi, and M. Takahashi, Jpn. J. Appl. Phys., Part 1 **38**, 4450 (1999).
[8]K. Macek, P. Macek, and U. Helmersson, Comput. Phys. Commun. **120**, 238 (1999).
[9]O. Yamazaki, K. Iyanagi, S. Takagi, and K. Nanbu, Jpn. J. Appl. Phys., Part 1 **41**, 1230 (2002).
[10]A. Kuzmichev and I. Goncharuk, IEEE Trans. Plasma Sci. **31**, 994 (2003).
[11]U. H. Kwon and W. J. Lee, Jpn. J. Appl. Phys., Part 1 **45**, 8629 (2006).
[12]S. Mahieu, G. Buyle, D. Depla, S. Heirwegh, P. Ghekiere, and R. De Gryse, Nucl. Instrum. Methods Phys. Res. B **183**, 313 (2006).
[13]R. S. Rossnagel, J. Vac. Sci. Technol. A **6**, 19 (1988).
[14]C. K. Birdsall and A. B. Langdon, *Plasma Physics via Computer Simulations* (Adam Hilger, Bristol, 1991).
[15]I. Kolev and A. Bogaerts, IEEE Trans. Plasma Sci. **34**, 886 (2006).
[16]I. Kolev, Ph.D. thesis, University of Antwerp, 2007.
[17]T. A. van der Straaten, N. F. Cramer, I. S. Falconer, and B. W. James, J. Phys. D: Appl. Phys. **31**, 177 (1988).
[18]I. Kolev, A. Bogaerts, and R. Gijbels, Phys. Rev. E **72**, 056402 (2005).
[19]E. Bultinck, I. Kolev, A. Bogaerts, and D. Depla, J. Appl. Phys. **103**, 013309 (2008).
[20]N. Matsunami *et al.*, At. Data Nucl. Data Tables **31**, 1 (1984).
[21]P. Sigmund, *Chapter Sputtering by Particle Bombardment in Topics in Applied Physics*, edited by I. R. Berhrisch (Springer, Berlin, 1981), Vol. 47.
[22]P. Sigmund, Phys. Rev. **184**, 383 (1969).
[23]M. W. Thompson, Philos. Mag. **18**, 377 (1968).
[24]J. Lindhard, M. Scharff, and H. E. Schiøtt, Mat. Fys. Medd. K. Dan. Vidensk. Selsk. **33**, 3 (1963).
[25]J. Sielanko, Radiat. Eff. Lett. Sect. **86**, 185 (1984).
[26]O. B. Firsov, Zh. Eksp. Teor. Fiz. **33**, 696 (1957).
[27]Z. Wronski, Vacuum **42**, 635 (1991).
[28]G. Buyle, (private communications).
[29]N. Baguer, Ph.D. thesis, University of Antwerp, 1996.
[30]A. Bogaerts and R. Gijbels, J. Appl. Phys. **79**, 1279 (1996).
[31]A. Bogaerts and R. Gijbels, Anal. Chem. **68**, 2676 (1996).
[32]N. Baguer and A. Bogaerts, J. Appl. Phys. **98**, 033303 (2005).
[33]J. Li, Q. Chen, and Z. Li, J. Phys. D: Appl. Phys. **28**, 1121 (1995).